Title

Study of pore pressure variation during liquefaction using two constitutive models for sand

Journal

Soil Dynamics and Earthquake Engineering, 27(1)

ISSN

0267-7261

Authors

Taiebat, Mahdi
Shahir, Hadi
Pak, Ali

Publication Date

2007

Peer reviewed

Published in Soil Dynamics and Earthquake Engineering, Vol. 27, No. 1, pages 60–72, 2007
doi:10.1016/j.soildyn.2006.03.004

STUDY OF PORE PRESSURE VARIATION DURING LIQUEFACTION USING TWO CONSTITUTIVE MODELS FOR SAND

Mahdi Taiebat [a,*], Hadi Shahir [b], Ali Pak [b]

[a] *Department of Civil and Environmental Engineering, University of California, Davis, One Shields Avenue, Davis, CA 95616, USA*

[b] *Department of Civil Engineering, Sharif University of Technology, P.O. Box 11365-9313, Tehran, Iran*

ABSTRACT

Numerical analyses of liquefiable sand are presented in this paper. Liquefaction phenomenon is an undrained response of saturated sandy soils when they are subjected to static or dynamic loads. A fully coupled dynamic computer code is developed to predict the liquefaction potential of a saturated sandy layer. Coupled dynamic field equations of extended Biot's theory with u-p formulation are used to determine the responses of pore fluid and soil skeleton. Generalized Newmark method is employed for integration in time. The soil behavior is modeled by two constitutive models; a critical state two-surface plasticity model, and a densification model. A class 'B' analysis of a centrifuge experiment is performed to simulate the dynamic response of level ground sites. The results of the numerical analyses demonstrate the capability of the critical sate two-surface plasticity model in producing pore pressures that are consistent with observations of the behavior of liquefiable sand in the centrifuge test.

Keywords: Fully coupled analysis, Finite element, Constitutive model, Bounding surface, Critical state, Plasticity, Densification, Liquefaction.

* Corresponding author. Tel.: +1-530-752-9589; Fax: +1-530-752-7872.
E-mail address: mtaiebat@ucdavis.edu (M. Taiebat).

Published in Soil Dynamics and Earthquake Engineering, Vol. 27, No. 1, pages 60–72, 2007
doi:10.1016/j.soildyn.2006.03.004

1. INTRODUCTION

Liquefaction is a term used frequently to describe a particular type of failure of saturated soils when they are subjected to static or cyclic loading. The interaction of soil and pore fluid under loading may lead to the build up of pore pressure, which results in material softening and loss of shear strength. In extreme case the soil loses all the shearing resistance and fails like a viscous liquid, a phenomenon known as 'liquefaction'. Liquefaction occurs frequently in saturated loose granular materials under earthquake and other dynamic loadings such as blast.

Loose granular materials such as sands are susceptible to compaction under vibration or cyclic loading. However, the reduction in volume is often prevented by lack of drainage, due to relatively low permeability, long drainage path or high frequency of load, during the period of vibration. Hence, a nearly undrained conditions prevail which result in build up of pore pressures to counter such contractive behavior. This causes reduction of the effective stress and eventually, for loose sands, may lead to a failure termed 'initial liquefaction', that is the state of zero effective stress in the soil. On the other hand, for a denser material, the state of zero effective stress state may never occur, and cycles of alternative contraction and dilation may take place, which is termed 'cyclic mobility' [1].

Quantitative analysis of liquefaction can only be accomplished by considering the coupled interaction of the soil skeleton and of the pore fluid. For this purpose, a suitable formulation for the behavior of the two-phase continuum and a proper constitutive model is required. In this paper, Biot's modified theory [2] is employed for modelling the saturated soil behavior and two plasticity models, namely a critical state two-surface plasticity model [3] and a densification model [4], are used as the constitutive models for sand.

Published in Soil Dynamics and Earthquake Engineering, Vol. 27, No. 1, pages 60–72, 2007
doi:10.1016/j.soildyn.2006.03.004

2. GENERAL FORMULATION

There are several different approaches to model the behavior of a two-phase medium. Generally, they can be classified as uncoupled and coupled analyses. In the uncoupled analysis, the response of saturated soil is modeled without considering the effect of soil-water interaction, and then the pore water pressure is included separately by means of a pore pressure generation model. In the coupled analysis a formulation is used where all unknowns are computed simultaneously at each time step. This is a more realistic representation of the physical phenomena than that provided by uncoupled formulation.

For a fully coupled analysis, equilibrium or momentum balance for the soil-fluid mixture, momentum balance for the fluid phase, and finally mass balance for the whole system of soil and fluid must be satisfied. The unknowns in this complete set of equations are displacement of solid phase (u_s), displacement of fluid phase relative to the solid phase (u_{rf}), and pressure of fluid phase (P). It is convenient to reduce the number of variables by neglecting the terms that have little influence on the results. For dynamic problems in which high-frequency oscillations aren't important, such as problems under earthquake loading, the relative velocity of fluid phase has little influence on the system and can be eliminated [5]. Therefore, the equations for fluid momentum balance and mass balance can be mixed together and as a result the governing equations are reduced to two. The primary variables in this form of equations are solid displacement and fluid pressure. Thus, this form is called u_s-P or for simplicity u-P formulation. The contribution of the solid acceleration in the equation of momentum balance of the fluid phase will render the final system of equations non-symmetric and can give unstable solutions in some cases [6]. This contribution has little effect on the system [7] and can be neglected.

Published in Soil Dynamics and Earthquake Engineering, Vol. 27, No. 1, pages 60–72, 2007
doi:10.1016/j.soildyn.2006.03.004

Using the finite element method for spatial discretization, the u-P formulation with the above mentioned simplification is as follows:

$$M\ddot{\overline{\mathbf{u}}} + \int_v B^T \boldsymbol{\sigma}\, dV - Q\overline{\mathbf{P}} - \mathbf{f}^{(1)} = 0 \tag{1}$$

$$Q^T \dot{\overline{\mathbf{u}}} + H\overline{\mathbf{P}} + S\dot{\overline{\mathbf{P}}} - \mathbf{f}^{(2)} = 0 \tag{2}$$

where M is the mass matrix, $\overline{\mathbf{u}}$ is the solid displacement vector, B is the strain-displacement matrix, $\boldsymbol{\sigma}$ is the effective stress tensor (determined by soil constitutive model which will be discussed later), Q indicates the discrete gradient operator coupling the motion and flow equations, $\overline{\mathbf{P}}$ is the pore pressure vector, S is the compressibility matrix, and H is the permeability matrix. The vectors $\mathbf{f}^{(1)}$ and $\mathbf{f}^{(2)}$ include the effects of body forces and prescribed boundary conditions. In Eq. (1), which represents continuity of motion, the first term represents the inertia force of the mixture followed by the internal force due to soil skeleton deformation, and by the internal force due to pore-fluid pressure. In Eq. (2), which is the equation for flow of fluid, the first and third terms represent the rate of volume change for the soil skeleton and the fluid phase, respectively, and the second term is the rate of pore fluid seepage.

In a numerical solution to the Eqs (1) and (2), it is necessary to integrate the equations in the time domain. Here, the generalized Newmark method is used [8] for this purpose. By employing this method and choosing $\Delta\overline{\mathbf{u}}_n$ and $\Delta\overline{P}_n$ as primary unknowns, the final set of equations is obtained as follows:

$$\left(\frac{1}{\alpha}\times M + \frac{\delta}{\alpha}\times\Delta t\times C\right)\Delta\overline{\mathbf{u}}_n - \left(\Delta t^2\times Q\right)\Delta\overline{\mathbf{P}}_n + \int_V B^T\boldsymbol{\sigma}_{n+1}dV\times\Delta t^2 - \mathbf{f}_{n+1}^{(1)} = 0 \tag{3}$$

$$\left(\frac{\delta}{\alpha}\times Q^T\right)\Delta\overline{\mathbf{u}}_n + \left(\Delta t\times H + \frac{1}{\theta}\times S\right)\Delta\overline{\mathbf{P}}_n - \mathbf{f}_{n+1}^{(2)} = 0 \tag{4}$$

Published in Soil Dynamics and Earthquake Engineering, Vol. 27, No. 1, pages 60–72, 2007
doi:10.1016/j.soildyn.2006.03.004

where α, δ and θ are the parameters of the generalized Newmark method and Δt is the time step. The vectors $\mathbf{f}_{n+1}^{(1)}$ and $\mathbf{f}_{n+1}^{(2)}$ can be evaluated explicitly from the information available at time t_n.

3. OUTLINE OF THE CONSTITUTIVE MODELS

Development of plasticity models that accurately simulate the behavior of engineering materials has been of great interest to engineers in recent years. In the case of geomaterials such as granular soils, the mathematical formulation of appropriate plasticity models is rather complex. It requires pressure sensitivity of the elastic bulk and shear moduli, third stress invariant dependence and in some cases two or multi-surface plasticity formulations. Moreover, to be useful in engineering calculations these complex models require efficient and robust numerical implementation.

In the numerical analyses presented in this paper two different constitutive models for granular soils have been employed and their results are compared. The first one is an advanced critical state two-surface plasticity model developed by Manzari and Dafalias [3] and the second constitutive model is a simple classical elastoplastic model called the densification model originally developed by Zienkiewicz et al. [4]. These models are briefly described in the following sections.

3.1 The critical state two-surface plasticity model

The formulation of the model is based on the general two-surface plasticity and the bounding surface plasticity theory. The state parameter, ψ, is used as the key ingredient to accurately model the effect of critical state for sands. In this model the strength and volume change behavior of the

Published in Soil Dynamics and Earthquake Engineering, Vol. 27, No. 1, pages 60–72, 2007
doi:10.1016/j.soildyn.2006.03.004

material are governed by the combined effect of density (void ratio) and confining stress. This combined effect is often represented by state parameter, $\psi = e - e_c$, where e_c is the critical void ratio corresponding to the existing confining stress on the soil element. When sheared in monotonic loading, granular soil that is denser than a critical state will exhibit a peak strength and upon further shearing a softening regime will appear in the stress-strain relationship. Granular soils with a void ratio more than their critical void ratio show a prevalent contractive response upon shearing toward critical state. A schematic representation of the two-surface model in the π-plane is shown in Figure 1.

The numerical efficiency of the model is good because only the yield surface must be updated at each increment, owing to kinematic and isotropic hardening. The other surfaces are fully determined by the value of state parameter ψ. A brief description of the basic equations of the model is given below [3,9]:

Elastic moduli

The elastic moduli, K and G, are defined through the following standard relationships:

$$\dot{\boldsymbol{\varepsilon}}_q^e = \frac{\dot{\mathbf{s}}}{2G}\ ,\ \dot{\varepsilon}_v^e = \frac{\dot{p}}{K} \tag{5}$$

where $\dot{\boldsymbol{\varepsilon}}_q^e$ and $\dot{\varepsilon}_v^e$ are the elastic components of the deviatoric and the volumetric strain increments, respectively, and $\dot{\mathbf{s}}$ and $\dot{p}$ are the deviatoric and the mean effective stress increment tensor. The isotropic hypoelasticity assumption is adopted, giving:

$$K = K_0\left(\frac{p}{p_{at}}\right)^a\ ,\ G = G_0\left(\frac{p}{p_{at}}\right)^a \tag{6}$$

Published in Soil Dynamics and Earthquake Engineering, Vol. 27, No. 1, pages 60–72, 2007
doi:10.1016/j.soildyn.2006.03.004

where p_{at} is the atmospheric pressure used as a reference pressure, for which $K = K_0$ and $G = G_0$, and a is a properly defined exponent yielding the variation of G and K with p.

Yield function

The shape of the yield surface is a cone with circular cross section in π plane, defined by:

$$F(\boldsymbol{\sigma}, \boldsymbol{\alpha}, m) = \sqrt{(\mathbf{s} - p\boldsymbol{\alpha}) : (\mathbf{s} - p\boldsymbol{\alpha})} - \sqrt{2/3}mp = 0 \tag{7}$$

In the above equation $\mathbf{s}$ is the deviatoric stress tensor, p and m represent the mean effective stress and the size of the yield surface respectively, and the back-stress ratio deviatoric tensor $\boldsymbol{\alpha}$ determines the position of the axis of the cone.

The loading direction is defined as the normal to the yield surface and given by:

$$\mathbf{L} = \frac{\partial F}{\partial \boldsymbol{\sigma}} = \mathbf{n} - \frac{1}{3} N \mathbf{I} \tag{8}$$

where $\mathbf{n} = \dfrac{\mathbf{r} - \boldsymbol{\alpha}}{\sqrt{2/3}m}$, $N = \boldsymbol{\alpha} : \mathbf{n} + \sqrt{2/3}m = \mathbf{n} : \mathbf{r}$, $\mathbf{r} = \dfrac{\mathbf{s}}{p}$ and $\mathbf{I}$ is the second rank identity tensor.

Flow rule

The plastic strain component is given by:

$$\dot{\boldsymbol{\varepsilon}}^p = \langle \lambda \rangle \frac{\partial Q}{\partial \boldsymbol{\sigma}} = \langle \lambda \rangle \left(\mathbf{n} + \frac{1}{3} D \mathbf{I} \right) \tag{9.1}$$

where Q is the plastic potential surface and D a dilatancy coefficient. In general D is not equal to N, which leads to a 'non-associated flow rule' ($F \neq Q$). λ is a loading index enclosed by the Macauley brackets $\langle\ \rangle$ to indicate loading, unloading, or neutral loading and is defined by:

Published in Soil Dynamics and Earthquake Engineering, Vol. 27, No. 1, pages 60–72, 2007
doi:10.1016/j.soildyn.2006.03.004

$$\lambda = \frac{1}{K_p}\left(\frac{\partial F}{\partial \boldsymbol{\sigma}} : \dot{\boldsymbol{\sigma}}\right) = \frac{2G\mathbf{n} : \dot{\boldsymbol{\varepsilon}}_q - KN\dot{\varepsilon}_v}{K_p + 2G - KDN} \tag{9.2}$$

where K_p is the plastic modulus.

Stress-rate expression

Using the additive decomposition, the increment of stress can be found in terms of total strain rates of $\dot{\boldsymbol{\varepsilon}}_q$ and $\dot{\varepsilon}_v$ as:

$$\begin{aligned}\dot{\boldsymbol{\sigma}} &= \dot{\mathbf{s}} + \dot{p}\mathbf{I} = 2G\dot{\boldsymbol{\varepsilon}}_q^e + K\dot{\varepsilon}_v^e\mathbf{I} \\ &= 2G(\dot{\boldsymbol{\varepsilon}}_q - \dot{\boldsymbol{\varepsilon}}_q^p) + K(\dot{\boldsymbol{\varepsilon}}_v - \dot{\boldsymbol{\varepsilon}}_v^p)\mathbf{I} \\ &= 2G\dot{\boldsymbol{\varepsilon}}_q + K\dot{\varepsilon}_v\mathbf{I} - \langle\lambda\rangle(2G\mathbf{n} + KD\mathbf{I})\end{aligned} \tag{10}$$

Bounding surface and dilatancy surface

The critical state of granular soil and its tendency for volume change are highly dependent on the direction of the stress path to which the soil is subjected. This can be achieved using the modified Lode angle θ as:

$$\cos 3\theta = \frac{3\sqrt{3}}{2}\left(\frac{\bar{S}}{\bar{J}}\right)^3 \tag{11.1}$$

in which:

$$\bar{J} = \left[\frac{1}{2}tr\bar{\mathbf{r}}^2\right]^{1/2},\ \bar{S} = \left[\frac{1}{3}tr\bar{\mathbf{r}}^3\right]^{1/3},\ \bar{\mathbf{r}} = \mathbf{r} - \boldsymbol{\alpha} \tag{11.2}$$

The bounding surface, dilatancy surface, and critical surface are defined in the following forms:

$$\boldsymbol{\alpha}_\theta^{\mathrm{b,c,d}} = \sqrt{(2/3)}\alpha_\theta^a\mathbf{n} \tag{12.1}$$

Published in Soil Dynamics and Earthquake Engineering, Vol. 27, No. 1, pages 60–72, 2007
doi:10.1016/j.soildyn.2006.03.004

$$\alpha_\theta^b = g(\theta,c)M_c + g(\theta,c_b)k_c^b\langle -\psi\rangle - m \tag{12.2}$$

$$\alpha_\theta^d = g(\theta,c)M_c + g(\theta,c_d)k_c^d\psi - m \tag{12.3}$$

$$\alpha_\theta^c = g(\theta,c)M_c - m \tag{12.4}$$

The above equations involve M_c (the critical stress ratio) and the two model parameters, k_c^b and k_c^d, that are used to define the bounding and dilatancy surfaces on the compression side of the surfaces. In order to complete the definition of these surfaces, it is necessary to define M_e, k_e^b, and k_e^d that are the corresponding values on the extension side of these surfaces. Parameters c, c_b and c_d define the ratios between the values on the extension side of these surfaces to those on the compression side of the surfaces ($c = M_e/M_c$, $\mathrm{c_b} = k_e^b/k_c^b$, $\mathrm{c_d} = k_e^d/k_c^d$). The equation for $g(\theta,c)$ is chosen as $g(\theta,c) = 2c/\left((1+c)-(1-c)\cos 3\theta\right)$.

In the above equations, the state parameter, ψ, is used to incorporate the critical state stress-strain behavior of the sand. Considering a straight-line approximation for the $e_c - \ln p$ relationship, e_c is defined as $e_c = (e_c)_{ref} - \lambda \ln\left(p/p_{ref}\right)$. Here λ is the slope of the critical state line in the $e_c - \ln p$ plane and $(e_c)_{ref}$ is the critical void ratio corresponding to a reference pressure, p_{ref}.

Hardening laws

Both isotropic and kinematic hardenings are used in the model. The evolution equations for the size, m, and the location, $\boldsymbol{\alpha}$, of the yield surface are given as:

$$\dot{m} = -c_m\dot{e}^p = \langle\lambda\rangle c_m(1+e_0)D = \langle\lambda\rangle\overline{m} \tag{13.1}$$

Published in Soil Dynamics and Earthquake Engineering, Vol. 27, No. 1, pages 60–72, 2007
doi:10.1016/j.soildyn.2006.03.004

$$\dot{\boldsymbol{\alpha}} = \langle\lambda\rangle h(\boldsymbol{\alpha}_\theta^{\mathrm{b}} - \boldsymbol{\alpha}) = \langle\lambda\rangle h\mathbf{b} = \langle\lambda\rangle hb\boldsymbol{\mu}^{\mathrm{b}} = \langle\lambda\rangle\overline{\boldsymbol{\alpha}} \tag{13.2}$$

c_m is a model parameter and $\dot{e}^p = -(1+e_0)\dot{\varepsilon}_v^p$ is the rate of change of plastic void ratio. The tensor $\boldsymbol{\alpha}_\theta^b$ indicates the image of the current stress state on the bounding surface. The tensor $\boldsymbol{\mu}^b$ is a unit tensor in the direction of $\mathbf{b} = \boldsymbol{\alpha}_\theta^b - \boldsymbol{\alpha}$ which is defined in Figure 1 as the vector (actually a second rank tensor) connecting the current back stress to its image on the bounding surface, $\boldsymbol{\alpha}_\theta^b$. The function h in the evolution equation for back stress, $\boldsymbol{\alpha}$, is chosen based on the original proposition by Dafalias and Popov [10] for two-surface models, that is:

$$h = h_0 \frac{|\mathbf{b}:\mathbf{n}|}{b_{ref} - |\mathbf{b}:\mathbf{n}|} \tag{14.1}$$

In this equation, h_0 is a model parameter and b_{ref} is a reference value of $\mathbf{b}$ which is chosen as:

$$b_{ref} = 2\sqrt{(2/3)}\alpha_c^b \tag{14.2}$$

In addition to the isotropic and kinematic hardening laws defined above, a fabric tensor is used to facilitate the modelling of sand behavior in unloading. The evolution of the fabric tensor, $\mathbf{F}$, is described as:

$$\dot{\mathbf{F}} = -\langle L\rangle C_f \langle -D\rangle \left(F_{\max}\mathbf{n} + \mathbf{F}\right) \tag{15}$$

Here, $F_{\max}$ and C_f are model parameters.

Dilatancy coefficient

The dilatancy coefficient, D, is related to the distance from the dilatancy surface $\mathbf{d}$:

$$D = A(\boldsymbol{\alpha}_\theta^{\mathrm{d}} - \boldsymbol{\alpha}):\mathbf{n} = A\mathbf{d}:\mathbf{n} = Ad\boldsymbol{\mu}^{\mathrm{d}}:\mathbf{n} \tag{16}$$

Published in Soil Dynamics and Earthquake Engineering, Vol. 27, No. 1, pages 60–72, 2007
doi:10.1016/j.soildyn.2006.03.004

in which $A = A_0\left(1+\langle \mathbf{F}:\mathbf{n}\rangle\right)$, where A_0 is a positive model parameter and $\mathbf{F}$ is the fabric tensor that was defined before. The tensor $\boldsymbol{\alpha}_\theta^d$ indicates the image of the current stress state on the dilatancy surface, as defined earlier. $\boldsymbol{\mu}^d$ is a unit tensor in the direction of $\mathbf{d} = \boldsymbol{\alpha}_\theta^d - \boldsymbol{\alpha}$ and $\mathbf{n}$ is the deviatoric part of the unit normal to the yield surface at the current stress state (Figure 1).

Plastic modulus

It is now possible to have a specific expression for plastic modulus using the definitions of $\overline{m}$, $\overline{\boldsymbol{\alpha}}$ and D:

$$K_p = -\frac{\partial F}{\partial \boldsymbol{\alpha}}:\overline{\boldsymbol{\alpha}} - \frac{\partial F}{\partial m}:\overline{m} = p\left(h\mathbf{b}:\mathbf{n} + \sqrt{2/3}c_m(1+e_0)A\mathbf{d}:\mathbf{n}\right) \tag{17}$$

3.2 The densification model

The densification model is a simple constitutive model presented by Zienkiewicz et al. [4] to simulate the 'autogenous' shrinkage or densification of solid phase which is the essential cause of pore pressure during cyclic loading, where elastoplastic behavior of the soil skeleton is taken into account by a different mechanism.. The constitutive equation is written as:

$$\dot{\boldsymbol{\sigma}} = \mathbf{D}_{\mathbf{ep}}\left(\dot{\boldsymbol{\varepsilon}} - \dot{\boldsymbol{\varepsilon}}_0\right) \tag{18}$$

where $\mathbf{D}_{\mathbf{ep}}$ represents the elastoplastic behavior and $\dot{\boldsymbol{\varepsilon}}_0$ (which is called autogenous strain) shows the densification caused by cyclic loading. In general a non-associative Mohr-Coulomb model with zero dilatancy is assumed for the elastoplastic behavior. A law describes the autogenous volumetric strain as below:

$$\left(\dot{\varepsilon}_0\right)_v = \frac{-A}{1+B\kappa}\dot{\kappa} \tag{19}$$

Published in Soil Dynamics and Earthquake Engineering, Vol. 27, No. 1, pages 60–72, 2007
doi:10.1016/j.soildyn.2006.03.004

where A and B are model parameters and κ is damage quantity, defined as:

$$\dot{\kappa} = \exp(\gamma\theta)\dot{\xi} \tag{20}$$

Here, γ is another parameter of the model. The stress ratio θ is given by:

$$\theta = \frac{\sqrt{J_{2D}}}{p_0} \tag{21}$$

where J_{2D} is the second effective stress invariant and p_0 is the mean effective stress at the start of cyclic loading. In Eq. (20) $\dot{\xi}$ is the accumulated deviatoric strain increment given by:

$$\dot{\xi} = \left(\dot{\boldsymbol{\varepsilon}}_q : \dot{\boldsymbol{\varepsilon}}_q\right)^{\frac{1}{2}} \tag{22}$$

where $\dot{\boldsymbol{\varepsilon}}_q$ is the deviatoric strain increment.

As noted in equation (20), the densification model defines the quantity of densification as a function of history of shear strain and stress ratio. In this model cyclic movement causes only an accumulated plastic volumetric strain, i.e. excess pore pressure, and no reversal mechanism exists. The excess pore pressure, however, can dissipate due to flow of the water in porous media.

4. MODIFIED PISA® FINITE ELEMENT PROGRAM

In order to study the dynamic response of a saturated soil layer as an initial-boundary-value problem, a geotechnical finite element program, PISA®, has been used. The first version of this program was developed at the University of Alberta, known as SAGE [11]. Later a commercial version of this program was released under the name of PISA® [12]. In the current research the finite element PISA® program was modified to include a capability for a fully-coupled nonlinear dynamic analysis of saturated porous media as well as appropriate constitutive models suitable

Published in Soil Dynamics and Earthquake Engineering, Vol. 27, No. 1, pages 60–72, 2007
doi:10.1016/j.soildyn.2006.03.004

for liquefaction analysis [13-15]. In this code saturated soil is modeled as a two-phase material based on the Biot's theory for consolidation of a saturated porous medium [2]. The simplified numerical framework of this theory, the u-P formulation, is incorporated in the code. The constitutive models described in the previous section have also been implemented in PISA®. The performance of these models will be discussed in the following section.

5. EVALUATION OF MODEL PERFORMANCE

The calibration of the critical state two-surface plasticity model can be done on the basis of the results of conventional triaxial compression and extension tests [3]. To demonstrate the performance of the two-surface plasticity model, first, simulations of three hypothetical undrained triaxial tests on Nevada sand at different void ratios subjected to an initial confining pressure of 160 kPa are presented in Figure 2. A list of model constants for Nevada sand is presented in Table 1 [15]. It should be noted that the value of $(e_c)_{ref}$ in this table corresponds to $p_{ref} = 160$ kPa. The results indicate that the model captures the difference between the state denser than critical (e=0.79) and the state looser than critical (e=0.81, 0.85) which conforms with the experimental evidence. The state looser than critical shows the softening behavior, and the state denser than critical shows the hardening behavior which are expected under undrained loading conditions.

In case of cyclic loads, results of the laboratory tests conducted on Nevada sand by the Earth Technology Corporation in the course of Verification of Liquefaction Analysis by Centrifuge Studies (VELACS) project [16] were used for numerical simulations. The model constants are the same as what was presented in Table 1. Using the critical state two-surface plasticity model, an undrained cyclic triaxial test conducted at an initial void ratio of 0.65 (D_r=60%) has been

Published in Soil Dynamics and Earthquake Engineering, Vol. 27, No. 1, pages 60–72, 2007
doi:10.1016/j.soildyn.2006.03.004

simulated. The soil sample was first isotropically consolidated to a mean confinement p=80 kPa. After completion of consolidation, a compressive deviatoric stress (q_0=7.5 kPa) has been applied as an offset under undrained conditions prior to applying the cyclic load. Thereafter, a cyclic vertical loading was applied with the amplitude 29.6 kPa and the frequency of 1 Hz. Comparison between numerical simulation and laboratory data for cyclic stress path, excess pore water pressure generation, and cyclic stress-strain is presented in Figure 3. The last few cycles of the loading in the available data shows negative confining pressure which makes this part of the data unreliable. The numerical simulation has been performed for the first 12 cycles of the loading. In general, the model captures the gradual generation of excess pore pressure which shows the effective simulation of the volumetric behavior in this model. Some differences may be recognized between the measured and predicted results. A reason for these differences is that the predicted results are for the average soil properties whereas the measured results contain deviation from the average.

For evaluation of the performance of the densification model, it worth mentioning that, this model only considers the monotonic increase of autogenous strain which causes liquefaction. The performance of this model is examined by simulation of another undrained cyclic triaxial test conducted on Nevada sand at an initial void ratio of 0.74 (D_r=40%). The isotropic consolidation pressure has been p=40 kPa and the deviatoric stress offset under undrained conditions q_0=3.9 kPa. The amplitude and frequency of cyclic loading were 18.4 kPa and 1 Hz, respectively. The parameters used in the densification model are shown in table 2 [14]. The shear modulus at different confining pressures is determined as a function of mean effective stress as follows:

$$G = G_0 \left(\frac{p}{p_{at}} \right)^n \tag{23}$$

Published in Soil Dynamics and Earthquake Engineering, Vol. 27, No. 1, pages 60–72, 2007
doi:10.1016/j.soildyn.2006.03.004

where p_{at} is the atmospheric pressure, p is the mean effective stress, G is the shear modulus, G_0 is shear modulus at atmospheric pressure, and n is dimensionless material constant. The resonant column test has been used to calculate the constants G_0 and n. Friction angle has been obtained in the standard manner from the results of the monotonic triaxial or simple shear tests. The cohesion is considered zero. Soil parameters for the dilatant behavior are obtained from the undrained cyclic test data. Comparison between numerical simulation and laboratory data for cyclic stress path and excess pore water pressure generation is presented in Figure 4. The model predicts generation of excess pore pressure and occurrence of full liquefaction in the sample in the fifth loading cycle. The damage parameter (κ) defined by equation (20), becomes very large when liquefaction takes place and causes a sharp increase in pore pressure. Performance of the densification model in predicting the pore pressure values seems good despite the low rate of pore pressure generation at the initial cycles. The predicated strains, however, has not been reasonable and therefore not reported.

6. APPLICATION OF THE NUMERICAL MODEL FOR PREDICTION OF LIQUEFACTION

The numerical models described in the previous sections are used to simulate a centrifuge test on liquefiable sand. Class 'B' prediction of the experiment No. 1 of VELACS project [18] is considered here. In VELACS project, extensive researches have been conducted on centrifuge simulation and numerical modelling of a liquefiable soil under earthquake loading. A brief description of the project is given below.

Published in Soil Dynamics and Earthquake Engineering, Vol. 27, No. 1, pages 60–72, 2007
doi:10.1016/j.soildyn.2006.03.004

6.1 Description of the experiment

The experimental case selected here is the centrifuge experiment No. 1 conducted during the course of VELACS project by Taboada and Dobry [18] at Rensselaer Polytechnic Institute (RPI). This experiment has been conducted on a 20cm high horizontal uniform layer of Nevada sand, which is placed in a laminar box at a relative density of about 40%. The laminar box was constructed of rectangular aluminum rings assembled on top of each other with roller bearings in between. The purpose of using laminar box was to simulate the response of a semi-infinite sand layer during shaking. A sketch of the laminar box and the instrumentations used for this experiment is presented in Figure 5. The sand layer was fully saturated with water and spun at a centrifuge acceleration of 50g while excited horizontally at the base with the target prototype accelerogram shown in Figure 6. The vertical acceleration was considered to be zero.

6.2 Numerical modelling

Numerical modelling of the experiment No. 1 was performed in a prototype scale considering two-dimensional plane-strain conditions. 64 rectangular elements having 4 nodes for pore pressure variation and 8 nodes for displacement variation were used in a uniform finite mesh as shown in Figure 7. The laminar box was modelled with the constraint of lateral tied nodes. The displacements of nodes located at the same level on the lateral boundaries were restrained to have the same value. The nodes at the base of the finite element model were fixed in both horizontal and vertical directions. Dissipation of pore pressure was allowed to occur only through the surface of the sand layer; while the lateral boundaries and the base were kept impermeable. The effect of the lateral inertia of the rings was neglected in the analysis. Analyses

Published in Soil Dynamics and Earthquake Engineering, Vol. 27, No. 1, pages 60–72, 2007
doi:10.1016/j.soildyn.2006.03.004

were performed in two steps: a static analysis was performed to apply the gravitational forces due to self weight of the soil before seismic excitation. The resulted hydrostatic pressures of fluid and the stress state along a soil column were used as initial conditions for the subsequent dynamic analysis. The numerical integration parameters of the generalized Newmark method were selected to be $\alpha = 0.3025$, $\delta = 0.60$ and $\theta = 0.60$ for the dynamic analysis.

6.3 Numerical results and discussion

The liquefaction behavior of saturated sand has been numerically simulated using the fully coupled formulation and two different constitutive models. The results of the analyses are presented in the following sections.

Excess pore pressure

Figure 8 displays the predicted and measured pore pressures at nodes P5 to P8, located in different levels of sand layer as shown in Figures 5 and 7. Reported data by RPI shows that the measured pore pressure time histories at the same elevations are essentially identical thus verifying the one-dimensional behavior of the model [18]. As expected, the numerical simulation results the pore pressures in the left (P1 to P4) same as those in the center (P5 to P8) which are shown in Figure 8. The first 20 seconds of the time history of pore pressure variation are shown separately on Fig. 7(a) while the complete time history of pore pressure variation is depicted on Fig. 7(b). In this figures, along with three curves of pore pressure variations, dash-dotted lines represent $r_u = u_e / \sigma_v$ at different elevations (u_e is excess pore pressure, and σ_v is the initial vertical effective stress). The r_u lines indicate whether or not the generated pore pressure reaches the condition of zero effective stress or primary liquefaction state due to excitation at the base of

Published in Soil Dynamics and Earthquake Engineering, Vol. 27, No. 1, pages 60–72, 2007
doi:10.1016/j.soildyn.2006.03.004

the laminar box. The measured pore pressure time histories (RPI test) indicate that soil at the P1 and P2 levels is liquefied. At P3 level it is liquefied just for a short period of time and at the P4 level, liquefaction has not taken place. Numerical modelling using the densification model shows a state of liquefaction at all levels in the soil. Although the sharp increase in pore pressure resulted from this model at the onset of shaking does not match with the experimental results, the pore pressure dissipation (consolidation phase) matches well with the experimental results. On the other hand numerical results using the two-surface plasticity model reveals very good agreement with the experimental values. The liquefaction state was shown clearly at P1 and P2 levels and a state close to liquefaction was captured in level P3 just for a short time. Patterns of the initial increasing, leveling off, and then decreasing the pore pressure capture the lab results very well.

The constitutive models have been first calibrated as mentioned in the section 5, and then the value of permeability has been adjusted in each simulation to get the best fit to the centrifuge data at the consolidation phase. The sand permeability obtained from a constant head laboratory test, was $k=6.6\times10^{-5}$ m/sec. In view of the scaling laws applicable to centrifuge experiments [19] the prototype permeability should be 50k, i.e. 3.3×10^{-3}. The results with the densification model have been obtained by selecting $k=3.3\times10^{-3}$ m/sec, while the results with the two-surface plasticity model have been obtained by taking $k=13.5\times10^{-3}$ m/sec both in the prototype scale. The adjusted values for coefficient of permeability for the analysis with the two-surface plasticity model is about 4 time greater than 50k to get the best fit to the centrifuge data. It has been observed by previous investigators that the soil permeability obtained from the standard laboratory test is different from the in-flight permeability of the soil in a liquefying state. For example Jafarzadeh and Yanagisawa [20] have shown that the coefficient of permeability triples

Published in Soil Dynamics and Earthquake Engineering, Vol. 27, No. 1, pages 60–72, 2007
doi:10.1016/j.soildyn.2006.03.004

during shaking compared to its initial value. Regarding the densification model, the predictions are not very good. The issue with this model is its fast rise which is due to the crude dilatancy law used in the model. This impacts the dissipation part as well. Although numerical simulation with the two-surface plasticity model confirms that the coefficient of permeability during liquefaction becomes greater than that obtained under static conditions, yet the calibrated value may not necessarily represent the actual soil permeability. Comparing the numerical results with the measured pore pressure responses over time, as shown in Figure 8, shows that the predicted drainage process at P5 and P6 is faster and at P8 is slower than the experimental ones. At P7 the drainage processes of numerical and experimental results show a good agreement with each other. These observations indicate that the coefficient of permeability is not a stationary parameter during shaking as well as during drainage processes. Therefore using a constant value for permeability in a numerical analysis possesses an inherent pitfall by which the drainage can not be simulated in a desirable manner. It seems that the change of the coefficient of permeability at the end of shaking takes place in such a way that it increases at shallow depths and decreases at increased depths, although this warrant further investigations.

The drainage sequence starting from bottom to top is evident from Figure 8. This is also confirmed by the experimental results. The magnitude of the excess pore pressure would be higher at the bottom and lower at the top, causing a pore pressure gradient which results an upward flow. Due to this gradient, the excess pore pressure at the bottom of the sand layer would dissipate first as the sand particles at the bottom come into contact with each other. Hence, the excess pore pressures at locations P8 and P7 would dissipate before those at locations P5 and P6. For a better illustration of this phenomenon, contours of r_u in different time steps are shown in Figure 9 for simulation with the two-surface plasticity model. At t=1.0 sec the values of r_u

Published in Soil Dynamics and Earthquake Engineering, Vol. 27, No. 1, pages 60–72, 2007
doi:10.1016/j.soildyn.2006.03.004

increases with depth. This causes an upward dissipation of pore water pressure in the soil. But at t=1.2 sec, the value of r_u at shallow depths becomes greater than its value at increased depths. This indicates that the excess pore water pressure depends upon the contractive characteristics of sand and inflow/outflow of the pore water. Changes in the pattern of variation of r_u along the sand column reveal the extremely complicated behavior of the pore fluid during the liquefaction process. The stress paths depicted in Figure 10 show the typical mechanism of cyclic decrease in effective stress due to pore pressure build-up, captured using the two-surface plasticity model. For saturated medium-dense cohesionless soils, the presented dynamic excitation response demonstrates minor cyclic mobility effect under level ground conditions.

Horizontal displacements

Variations of horizontal displacement over time are shown in Figures 11 and 12. In Figure 11 the predicted displacements using the critical state two-surface plasticity model are compared with the laboratory results. Figure 12 displays the densification model predictions for the horizontal displacements.

In the predicted horizontal displacements using the two-surface plasticity model, the amplitudes of oscillations are smaller than the measured values. The predicted maximum values of displacements are also smaller than those measured. The final values of the horizontal displacement at LVDT3 & LVDT4 are simulated well. In general, good agreement is achieved between the computed and recorded responses.

The predicted values using the densification model are much larger than the measured values in the RPI test. As noted in the preceding section, numerical modelling using the densification model shows a state of liquefaction at all levels in the soil. However, liquefaction has not taken

Published in Soil Dynamics and Earthquake Engineering, Vol. 27, No. 1, pages 60–72, 2007
doi:10.1016/j.soildyn.2006.03.004

place at increased depths in the RPI test. Therefore, this residual displacement is probably due to small effective confining stress in the whole depth of the sand column.

Vertical displacements

The predicted and measured vertical displacement time histories at the free surface of the sand layer are presented in Figure 13. Predicted settlement is about 17 cm at LVDT1 using two-surface plasticity model. The predicated settlement using the densification model is virtually zero. Most of the settlements occur during the shaking period as also depicted by the experiment. The maximum predicted settlement has been found to be 17 cm which is in good agreement with the experimental observations, which is about 20 cm.

7. CONCLUSIONS

Liquefaction phenomenon of loose saturated sand layer in a laminar box in centrifuge experiment was simulated using a fully coupled set of dynamic equations with a u-P formulation and two types of plasticity models for sand. The results indicate that:

1. The densification model based on the classical elastoplastic framework can predict the liquefaction phenomenon close to ground surface, where the confining stresses are low, but it is unable to accurately predict this phenomenon at points deeper in the soil. The capability of the densification model in predicting the horizontal and vertical displacement during liquefaction process is relatively poor.
2. The critical state two-surface plasticity model captures most of the important features of the complex interaction of pore fluid and sand particles subjected to cyclic loads. Pore pressure variation and vertical displacements during liquefaction can be simulated with very good

Published in Soil Dynamics and Earthquake Engineering, Vol. 27, No. 1, pages 60–72, 2007
doi:10.1016/j.soildyn.2006.03.004

accuracy using this advanced plasticity model, which shows the superiority of using the model for simulation of liquefaction.

3. Liquefaction usually causes a significant increase of the coefficient of permeability, but rapid changes in the pattern of excess pore pressure in the soil column during shaking demonstrate that permeability is not a stationary parameter in the liquefaction process and it may either increase or decrease at different depths. Hence assumption of a constant value of the coefficient of permeability can not be regarded as a suitable approach. Finding a realistic assumption for variation of the coefficient of permeability during liquefaction requires further investigation.

ACKNOWLEDGEMENTS

The authors would like to sincerely thank Professor Majid T. Manzari and Professor Yannis F. Dafalias for their advice and guidance during this research.

Published in Soil Dynamics and Earthquake Engineering, Vol. 27, No. 1, pages 60–72, 2007
doi:10.1016/j.soildyn.2006.03.004

REFERENCES

[1] Pastor M, Chan AHC, Zienkiewicz OC. Constitutive and numerical modelling of liquefaction. In: Musharraf Zaman, Giancarlo Gioda and John Booker, editors. Modelling in Geomechanics. Chichester: Wiley, 2000; 91-128.

[2] Biot MA. General theory of three dimensional consolidation. Journal of Applied Physics 1941; 12(2): 155-164.

[3] Manzari MT, Dafalias YF. A critical state two-surface plasticity model for sands. Geotechnique 1997; 47(2): 255-272.

[4] Zienkiewicz OC, Chang CT, Hinton E. Non-linear seismic response and liquefaction. International Journal of Numerical and Analytical Methods in Geomechanics. 1978; 2: 381- 404.

[5] Zienkiewicz OC, Chan AHC, Pastor M, Schrefler BA, Shiomi T. Computational geomechanics with special reference to earthquake engineering. John Wiley & Sons, 1999.

[6] Park KC. Stabilization of partitioned solution procedures for pore-fluid interaction analysis. International Journal of Numerical Methods in Engineering 1983; 19: 1669- 1673.

[7] Zienkiewics OC, Chan AHC, Pastor M, Shiomi T. Computational approach to soil dynamics. In: Cakmak AS, editor. Soil Dynamics and Liquefaction. Elsevier, 1987.

[8] Katona MG, Zienkiewicz OC. A unified set of single step algorithms Part 3: The Beta-m method, a generalization of the Newmark scheme. International Journal of Numerical Methods in Engineering 1985; 21: 1345- 1359.

[9] Manzari MT, Prachathananukit R. On integration of a cyclic soil plasticity model. International Journal for Numerical and Analytical Methods in Geomechanics 2001; 25: 525-549.

Published in Soil Dynamics and Earthquake Engineering, Vol. 27, No. 1, pages 60–72, 2007
doi:10.1016/j.soildyn.2006.03.004

[10] Dafalias YF, Popov EP. Plastic internal variable formalism of cyclic plasticity. Journal of Applied Mechanics 1976; 98(4): 645-650.

[11] Chan D, Morgenstern N. SAGE: A finite element program for stress analysis in geotechnical engineering, Program User Manual. Geotechnical Group. The University of Alberta, 1988.

[12] Chan D. PISA: Program for incremental stress analysis. User Manual, version 1.0. PISA Inc, 1997.

[13] Pak A. Numerical modelling of hydraulic fracturing. PhD Thesis. Department of Civil and Environmental Engineering, University of Alberta, 1997.

[14] Shahir H. Dynamic analysis of saturated porous media for Numerical simulation of liquefaction. MSc Thesis. Department of Civil Engineering, Sharif University of Technology, 2001.

[15] Taiebat M. Application of a critical state two-surface plasticity model for numerical simulation of soil liquefaction with a fully coupled approach. MSc Thesis. Department of Civil Engineering, Sharif University of Technology, 2003.

[16] Arulmoli K, Muraleetharan KK, Hossain MM, Fruth LS. VELACS: Verification of Liquefaction Analyses by Centrifuge Studies - Laboratory Testing Program, Soil Data Report. Earth Technology Corporation; 1992. Also available from University of Southern California web site, http:rccgOl.usc.edu/eqdata/home.html.

[17] Shiomi T, Shigeno Y, Zienkiewicz OC. Numerical prediction for Model No. 1. In: Arulanandan K, Scott RF, editors.Verification of Numerical procedures for the analysis of soil liquefaction problems. Rotterdam: AA Balkema, 1993; 213- 219.

Published in Soil Dynamics and Earthquake Engineering, Vol. 27, No. 1, pages 60–72, 2007
doi:10.1016/j.soildyn.2006.03.004

[18] Taboada VM, Dobry R. Experimental results of Model No. 1 at RPI. In: Arulanandan K, Scott RF, editors. Verification of Numerical procedures for the analysis of soil liquefaction problems. Rotterdam: AA Balkema, 1993; 3-18.

[19] Tan TS, Scott RF. Centrifuge scaling considerations for fluid-particle systems. Geotechnique 1985; 35(4):461–470.

[20] Jafarzadeh F, Yanagisawa E. Settlement of sand models under unidirectional shaking. First International Conference on Earthquake Geotechnical Engineering. IS-Tokyo, 1995; 2: 693-698.

Published in Soil Dynamics and Earthquake Engineering, Vol. 27, No. 1, pages 60–72, 2007
doi:10.1016/j.soildyn.2006.03.004

Figure Captions:

Figure 1: Schematic representation of the two-surface model in π-plane [3]

Figure 2: Model simulation of three undrained triaxial tests at three different void ratios using the two-surface plasticity model (e_c=0.8 for p=160 kPa)

Figure 3: Model simulation of undrained cyclic triaxial test using the two-surface plasticity model, data for Nevada sand (e=0.65) [16]

Figure 4: Model simulation of undrained cyclic triaxial test using the densification model, data for Nevada sand (e=0.74) [16]

Figure 5: Cross-sectional view of the centrifuge laminar box

Figure 6: Horizontal input acceleration at the base of the laminar box

Figure 7: Finite element mesh and boundary conditions

Figure 8: Recorded and computed excess pore pressure time histories

Figure 9: Contours of computed r_u in different time steps (two-surface plasticity model)

Figure 10: Computed effective stress path at different depths (two-surface plasticity model)

Figure 11: Recorded and computed (two-surface plasticity model) lateral displacement time histories

Figure 12: Computed lateral displacement time histories (densification model)

Figure 13: Recorded and computed settlement time histories at the free surface of sand column

Published in Soil Dynamics and Earthquake Engineering, Vol. 27, No. 1, pages 60–72, 2007
doi:10.1016/j.soildyn.2006.03.004

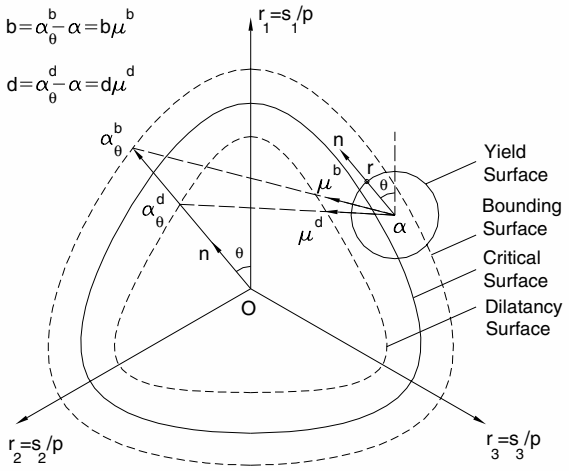

Figure 1: Schematic representation of the two-surface model in π-plane [3]

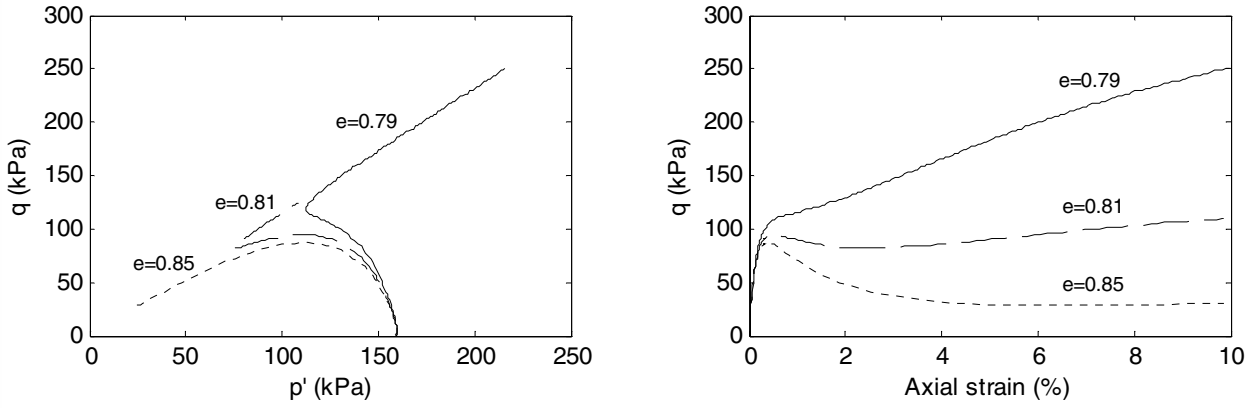

Figure 2: Model simulation of three undrained triaxial tests at three different void ratios using the two-surface plasticity model (e_c=0.8 for p=160 kPa)

Published in Soil Dynamics and Earthquake Engineering, Vol. 27, No. 1, pages 60–72, 2007
doi:10.1016/j.soildyn.2006.03.004

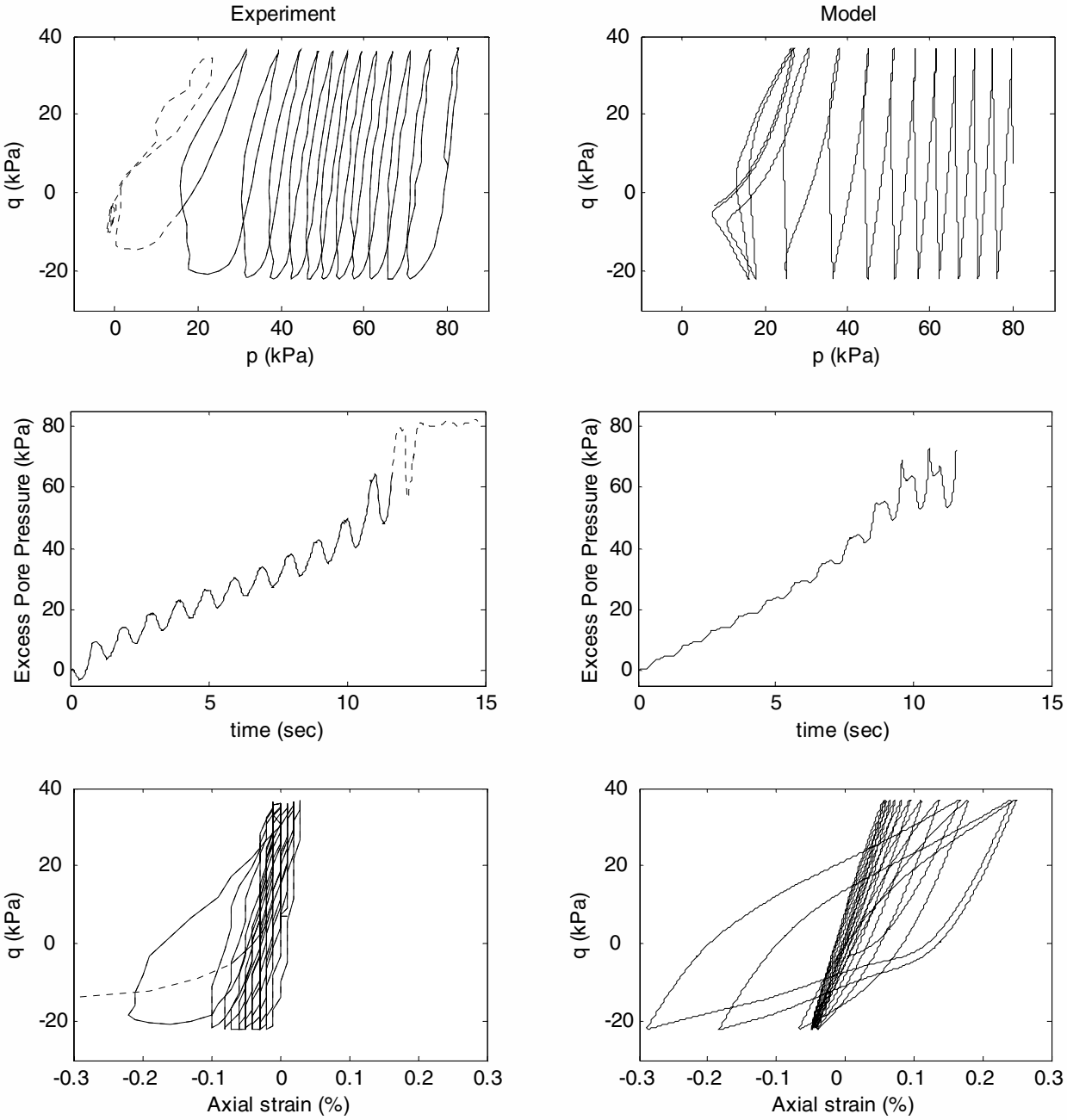

Figure 3: Model simulation of undrained cyclic triaxial test using the two-surface plasticity model, data for Nevada sand (e=0.65) [16]

Published in Soil Dynamics and Earthquake Engineering, Vol. 27, No. 1, pages 60–72, 2007
doi:10.1016/j.soildyn.2006.03.004

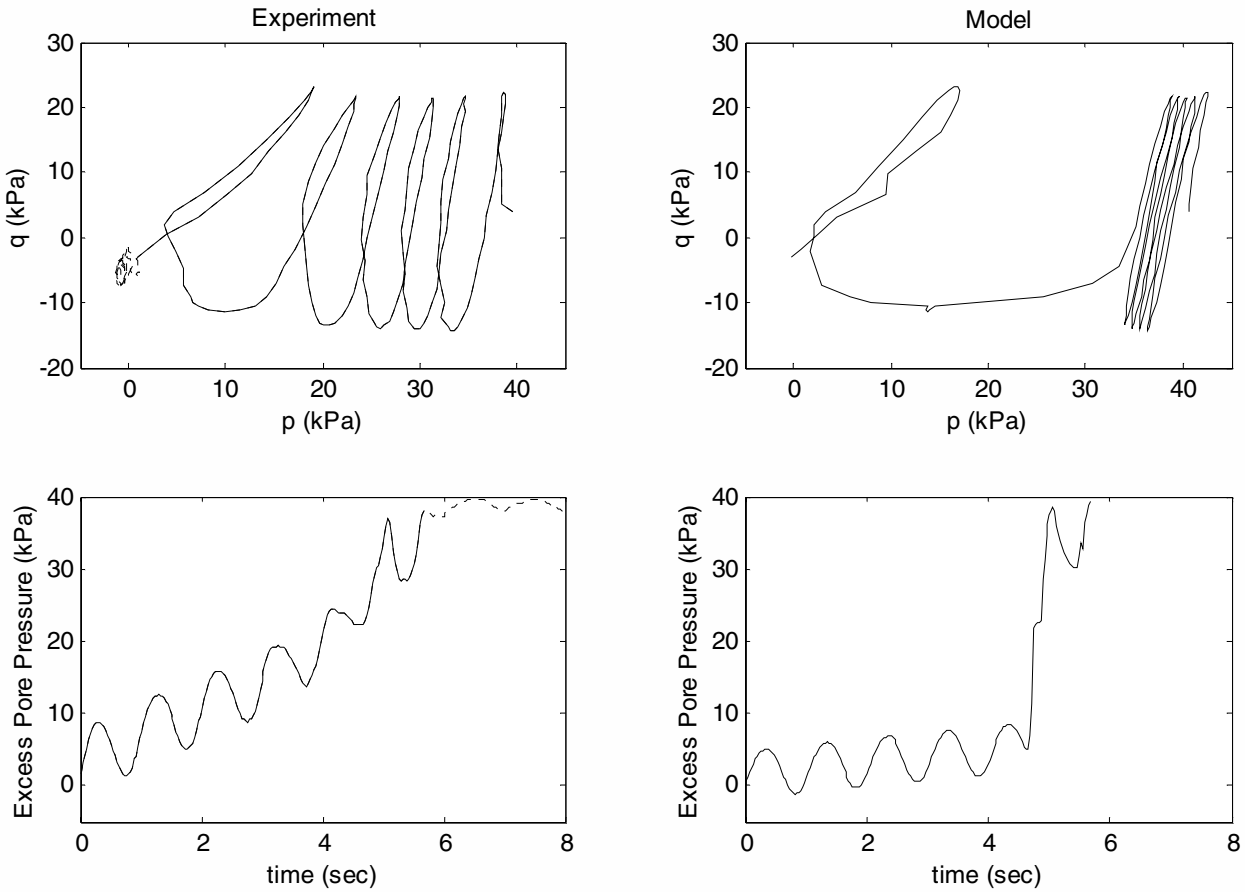

Figure 4: Model simulation of undrained cyclic triaxial test using the densification model, data for Nevada sand (e=0.74) [16]

Published in Soil Dynamics and Earthquake Engineering, Vol. 27, No. 1, pages 60–72, 2007
doi:10.1016/j.soildyn.2006.03.004

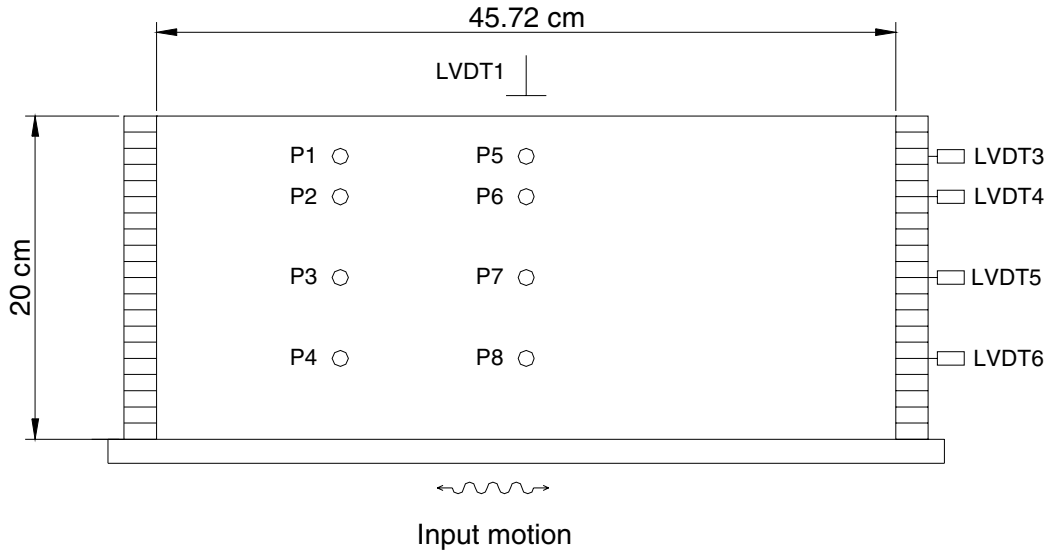

Figure 5: Cross-sectional view of the centrifuge laminar box

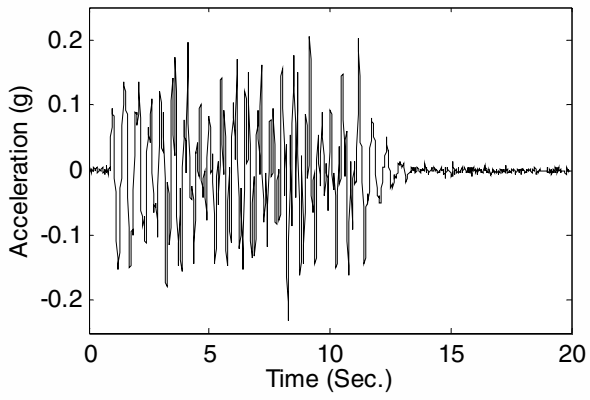

Figure 6: Horizontal input acceleration at the base of the laminar box

Published in Soil Dynamics and Earthquake Engineering, Vol. 27, No. 1, pages 60–72, 2007
doi:10.1016/j.soildyn.2006.03.004

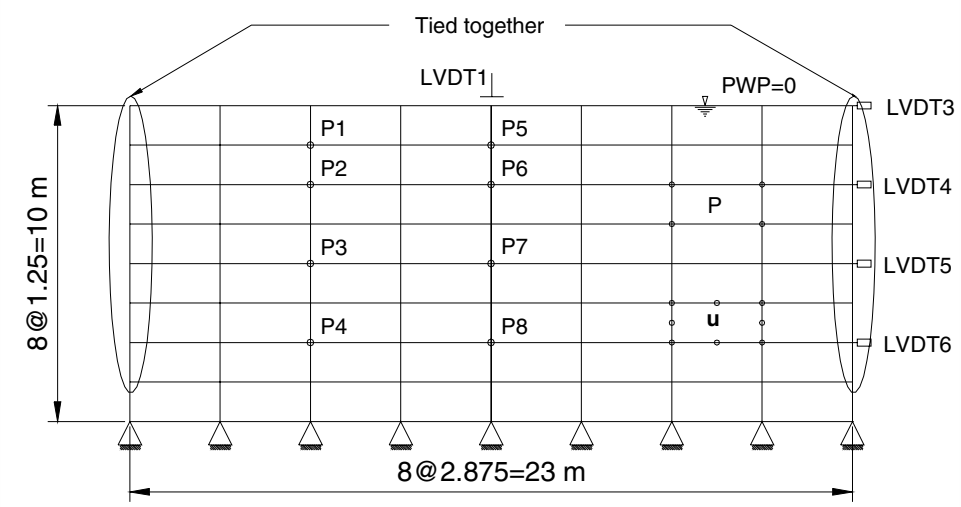

Figure 7: Finite element mesh and boundary conditions

Published in Soil Dynamics and Earthquake Engineering, Vol. 27, No. 1, pages 60–72, 2007
doi:10.1016/j.soildyn.2006.03.004

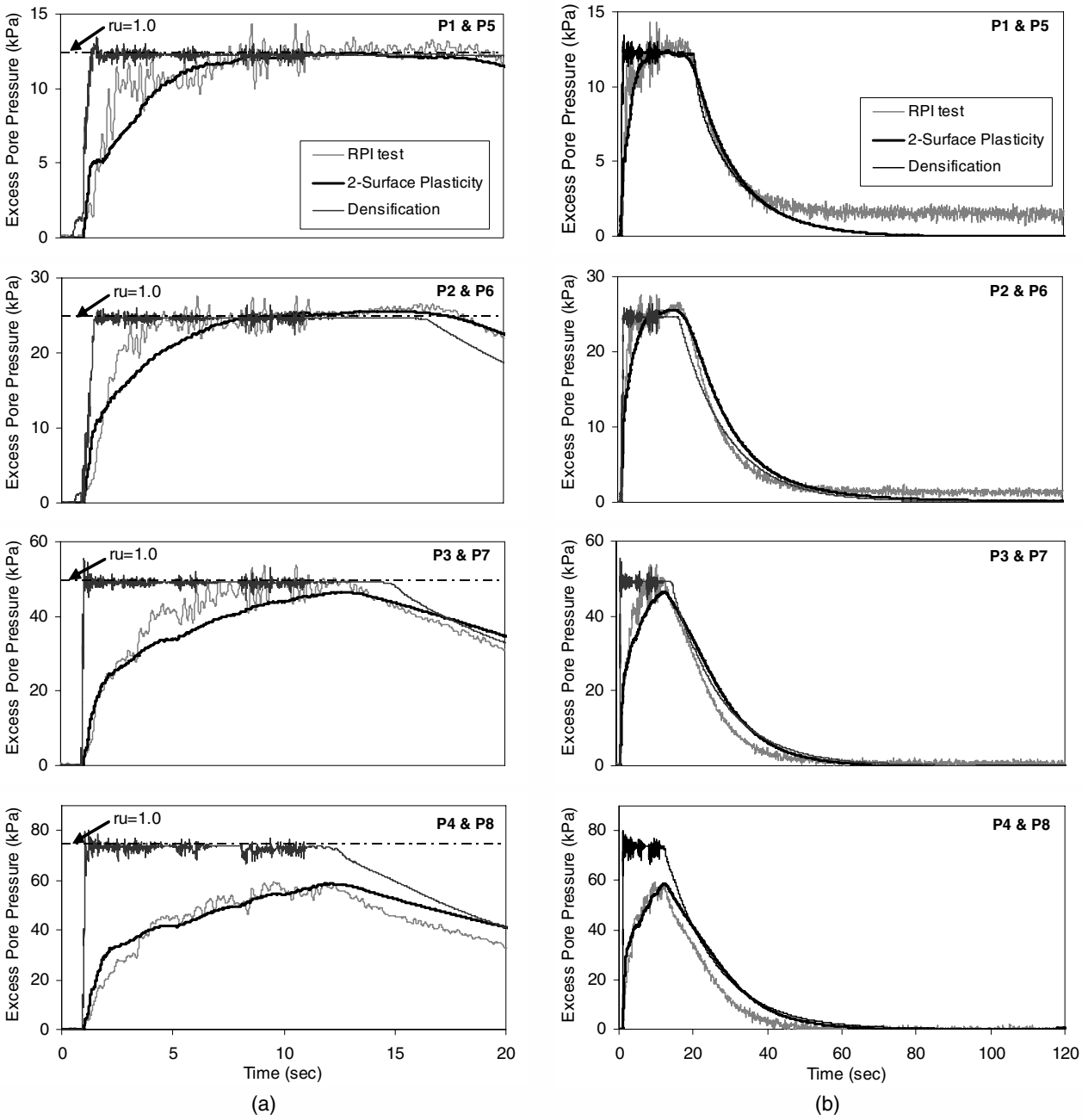

Figure 8: Recorded and computed excess pore pressure time histories

Published in Soil Dynamics and Earthquake Engineering, Vol. 27, No. 1, pages 60–72, 2007
doi:10.1016/j.soildyn.2006.03.004

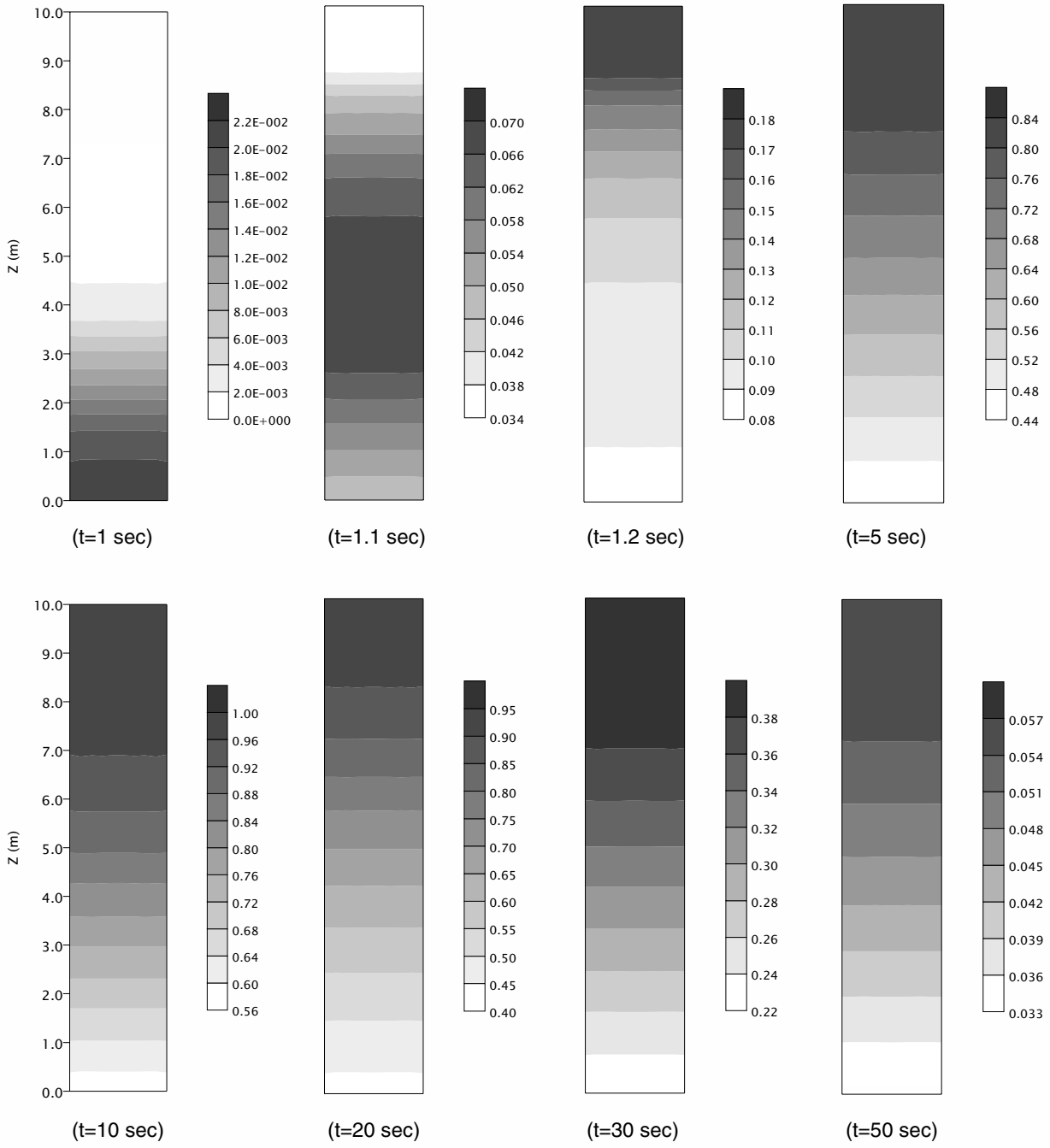

Figure 9: Contours of computed r_u in different time steps (two-surface plasticity model)

Published in Soil Dynamics and Earthquake Engineering, Vol. 27, No. 1, pages 60–72, 2007
doi:10.1016/j.soildyn.2006.03.004

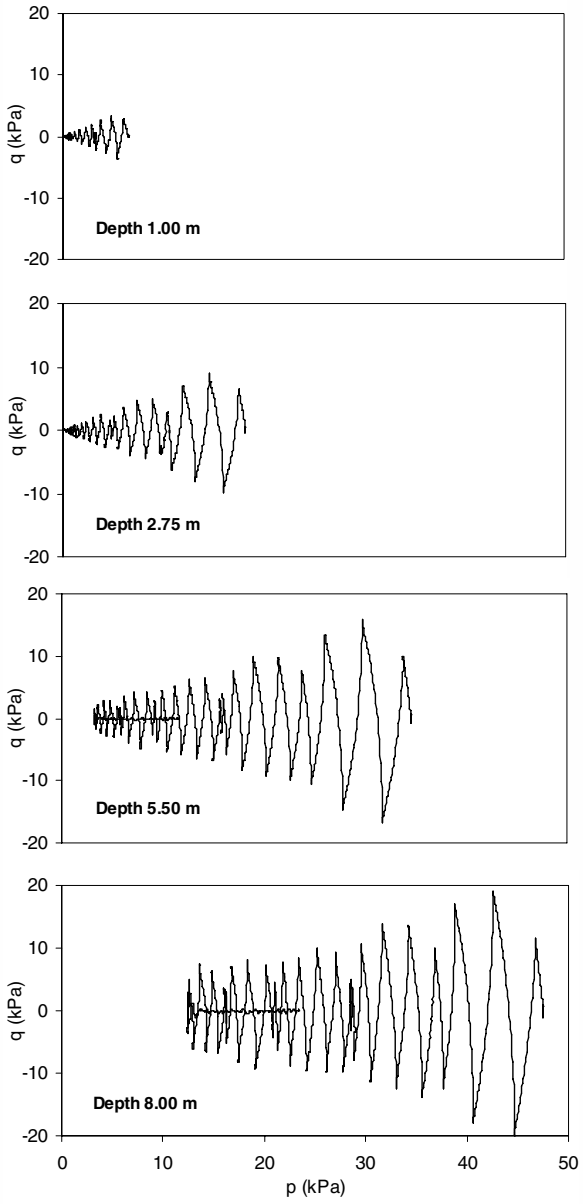

Figure 10: Computed effective stress path at different depths (two-surface plasticity model)

Published in Soil Dynamics and Earthquake Engineering, Vol. 27, No. 1, pages 60–72, 2007
doi:10.1016/j.soildyn.2006.03.004

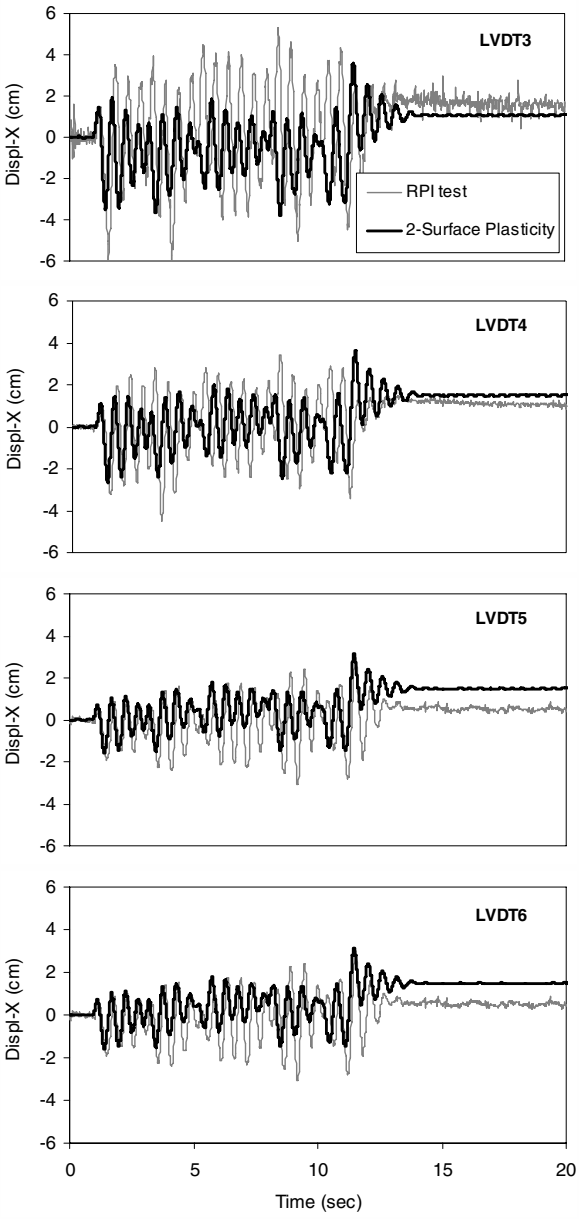

Figure 11: Recorded and computed (two-surface plasticity model) lateral displacement time histories

Published in Soil Dynamics and Earthquake Engineering, Vol. 27, No. 1, pages 60–72, 2007
doi:10.1016/j.soildyn.2006.03.004

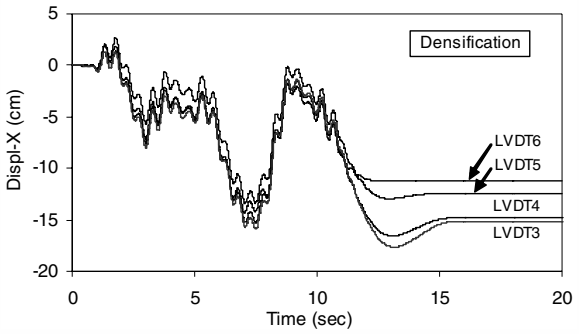

Figure 12: Computed lateral displacement time histories (densification model)

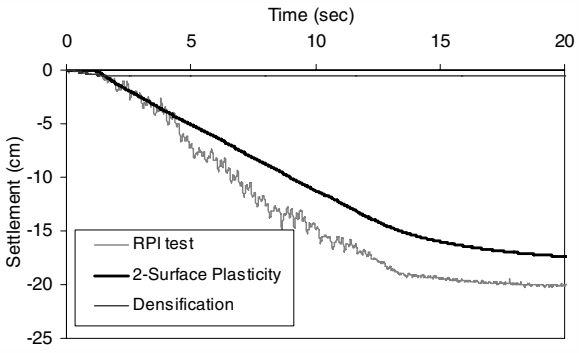

Figure 13: Recorded and computed settlement time histories at the free surface of sand column

Published in Soil Dynamics and Earthquake Engineering, Vol. 27, No. 1, pages 60–72, 2007
doi:10.1016/j.soildyn.2006.03.004

Table Captions:

Table 1: Material parameters of the critical state two-surface plasticity model for Nevada sand [15]

Table 2: Material parameter of the densification model for Nevada sand (Dr=40%) [14]

Published in Soil Dynamics and Earthquake Engineering, Vol. 27, No. 1, pages 60–72, 2007
doi:10.1016/j.soildyn.2006.03.004

Table 1: Material parameters of the critical state two-surface plasticity model for Nevada sand [15]

Elastic	G_0 (kPa)	31400	Hardening	h_0	800
	K_0 (kPa)	31400		m	0.05
	a	0.6		c_m	0.
Critical state	M_c	1.14	State parameter	k_c^b	3.975
	M_e	1.14		k_e^b	2.0
	λ	0.025		k_c^d	4.2
	$(e_c)_{ref}$	0.8		k_e^d	0.07
Dilatancy	A_0	0.6			
	C_f	100			
	$F_{\max}$	100			

Table 2: Material parameters of the densification model for Nevada sand (Dr=40%) [14]

Shear constant, G_0 (kPa)	73000
Shear exponent, n	0.5
Poisson's ratio, ν	0.31
Cohesion, c (kPa)	0.0
Friction angle, ϕ (deg)	34
Dilation angle, ψ (deg)	0.0
Densification parameter, γ	0.5
Densification parameter, A	0.05
Densification parameter, B	12.0